Spatial Resolution Limits for Needle Hydrophones From 0.5 to 20 MHz With Implications for Transcranial Ultrasound

Keith A. Wear, *Life Fellow, IEEE*, Christopher R. Fury, and Andre V. Alvarenga

***Abstract*—Hydrophone spatial resolution and spatial averaging effects are determined by the frequency-dependent effective sensitive element diameter $d_{\mathrm{eff}}(f)$ rather than the geometrical sensitive element diameter d_g. The objective of this work was to quantify average $d_{\mathrm{eff}}(f)$ for needle hydrophones as a function of d_g and f. Estimates of effective radii $a_{\mathrm{eff}}(f) = d_{\mathrm{eff}}(f)/2$ were inferred from directivity measurements from 0.5 to 20 MHz on 16 needle hydrophones with $d_g = 2a_g$ ranging from 75 to 1000 μm (139 hydrophone/frequency combinations). Effective sensitive element diameter $d_{\mathrm{eff}}(f)$ exceeded d_g by over 100% when $\lambda > 4d_g$ (where λ is the wavelength). For $ka_g > 0.75$ (where $k = 2\pi/\lambda$), $d_{\mathrm{eff}}(f)$ was consistent with the "rigid piston" (RP) theory, reinforcing a previous report from our laboratories. However, for $ka_g < 0.75$, $d_{\mathrm{eff}}(f)$ showed noticeable deviations from RP theory and fell between predictions from RP theory and predictions for an unbaffled (UB) circular piston. Examples: 1) for a needle hydrophone with $d_g = 75$ μm at 1 MHz ($ka_g = 0.16$), the data imply that average $d_{\mathrm{eff}} = 505$ μm, and 2) for a needle hydrophone with $d_g = 400$ μm at 500 kHz (common parameters for human transcranial neuromodulation; $ka_g = 0.42$), the data imply that average $d_{\mathrm{eff}} = 1215$ μm.**

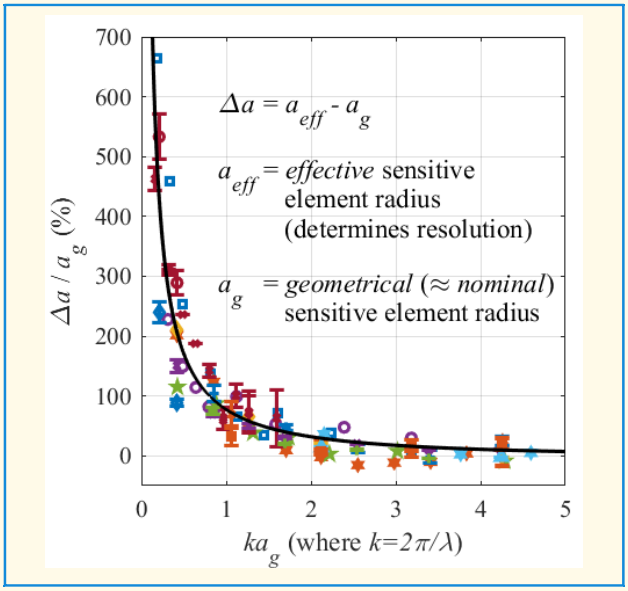

***Index Terms*—Directivity, effective sensitive element size, hydrophone, needle, resolution.**

I. Introduction

A. Nominal Versus Effective Hydrophone Sensitive Element Size

HYDROPHONES are used ubiquitously in medical ultrasound and nondestructive evaluation to measure acoustic pressure fields [1]. To properly interpret hydrophone-based pressure measurements, it is important to understand hydrophone spatial resolution limitations. Unfortunately, hydrophones do not always achieve spatial resolution near the nominal sensitive element size (approximately equal to the geometrical sensitive element size) [2]. This is because hydrophones perturb the pressure fields that they are used to measure, even when sensitive element sizes are much smaller than a wavelength. The gap between effective sensitive element diameter $d_{\mathrm{eff}}(f)$ (defined in IEC 62127-3 [3]) and nominal sensitive element diameter d_g is most noticeable at low frequencies [2]. Hydrophone frequency-dependent effective sensitive element size (i.e., spatial resolution) may be inferred from frequency-dependent directivity measurements [3].

Hydrophones can underestimate pressures and intensities due to spatial averaging effects across the sensitive element surface [4], [5], [6], [7], [8], [9], [10], [11], [12], [13], [14], [15], [16], [17], [18], [19]. When implementing algorithms for spatial averaging corrections, it is important to understand the effects of effective sensitive element size. Equations (20) and (21) in [12], which have been adopted in IEC 62127-1 [20], show the dependence of the spatial averaging factor on the frequency-dependent effective sensitive element size.

Frequency-dependent effective sensitive element sizes have been investigated for needle [21], [22], [23], [24], [25], [26], [27], membrane [21], [22], [23], [24], [26], [27], [28], [29], Fabry–Perot interferometric-type fiber optic [22], [30], reflectance-type fiber optic [31], and capsule [2], [27] hydrophones. Needle hydrophones are commonly used for

Received 3 August 2025; accepted 25 August 2025. Date of publication 16 September 2025; date of current version 1 December 2025. *(Corresponding author: Keith A. Wear.)*

Keith A. Wear is with United States Food and Drug Administration, Silver Spring, MD 20993 USA (e-mail: keith.wear@alumni.stanford.edu).

Christopher R. Fury and Andre V. Alvarenga are with the National Physical Laboratory, TW11 0LW Teddington, U.K. (e-mail: chris.fury@npl.co.uk; andre.alvarenga@npl.co.uk).

Digital Object Identifier 10.1109/TUFFC.2025.3610361

Highlights

- **Hydrophones perturb pressure fields, and consequently, their spatial resolution can be inferior to their geometrical sensitive element diameter d_g by 100% or more when $\lambda > 4d_g$ (where λ = wavelength).**
- **An empirical formula has been obtained to enable researchers to easily estimate and report the effective sensitive element diameter of their needle hydrophone at their operating frequency.**
- **Needle (and capsule) hydrophones conform closely to "rigid piston" (RP) theory when $\lambda < 4d_g$ and fall between RP theory and theory for an unbaffled (UB) circular piston when $\lambda > 4d_g$.**

biomedical applications because they are relatively portable and inexpensive [1]. Moreover, their small cross sections (e.g., compared to membrane hydrophones) reduce the potential for reflections that can adversely affect measurements (particularly when extended tone bursts rather than short broadband pulses are used) [1].

B. Low-Frequency Regime

The low-frequency regime (e.g., $\lambda > d_g/2$), where the gap between effective and nominal sensitive element sizes is particularly prominent, has become increasingly important in recent years due to increasing activity in transcranial ultrasound for thermal ablation [32], [33], blood brain barrier opening [34], [35], [36], and neuromodulation [37], [38], for which frequencies are often below 1 MHz. For example, for a hydrophone with a nominal sensitive element diameter of 400–500 μm and a frequency of 500 kHz (common parameters for transcranial neuromodulation in humans [39], [40], [41], [42], [43], [44], [45] and animals [39], [46], [47], [48], [49], [50], [51]), λ/d_g ranges from 5.9 to 7.4. Low frequencies are used to minimize distortions due to skull, which has nonplanar interfaces and high sound-speed mismatches with soft tissues. A recent consensus paper of the International Transcranial Ultrasonic Stimulation Safety and Standards Consortium (ITRUSST) notes that for many transcranial applications, "the effective size of the hydrophone sensitive area can be significantly larger than the nominal size" and encourages researchers to be conscious of this when selecting a hydrophone for system characterization measurements (Supplementary Material, Section B2 [37]).

C. Objectives of This Investigation

The main objective of this article is to obtain an empirical relation for needle hydrophone average effective sensitive element size (i.e., spatial resolution) as a continuous function of nominal sensitive element size and frequency, with emphasis on the low-frequency regime. (At high frequencies, effective sensitive element size asymptotically approaches the geometrical sensitive element size [2].) Here, new frequency-dependent effective sensitive element size measurements on seven needle hydrophones are reported and pooled with previously published data from our [25] and three other [22], [26], [27] laboratories to result in a dataset of 16 needle hydrophones interrogated over the frequency range from 0.5 to 20 MHz.

In addition, to elucidate physical mechanisms underlying the operation of needle hydrophones, empirical frequency-dependent effective sensitive element sizes are interpreted in the context of the "rigid piston" (RP) model [52] and the "unbaffled" (UB) circular piston model [21], [53]. The RP model was previously shown by our laboratories to be consistent with directivity data from a set of four needle hydrophones at traditional diagnostic ultrasound frequencies ($\geq$1 MHz) [25].

The novel aspects of this investigation are as follows. First, by pooling data for 16 needle hydrophones, greater levels of statistical confidence and generalizability are obtained compared with previous studies that utilized no more than four needle hydrophones. Second, by pooling measurements from four laboratories, conclusions are less dependent, compared with previous studies, on any particular laboratory's experimental methodology. Third, by including data from the two leading manufacturers of needle hydrophones, rather than just one as in previous studies, potential effects due to differences in design and manufacturing processes can be elucidated. Fourth, by paying particular attention (in both data collection and analysis) to the low-frequency regime, the implications of the results may be considered in the context of the rapidly emerging field of transcranial ultrasound, which may not have been fully anticipated in previous studies. Finally, by comparing the predictions of RP and UB models to empirical data for needle hydrophones at low frequencies: 1) our fundamental understanding of the physics of needle hydrophones is advanced and 2) the accuracy of corresponding methodology for correcting for frequency-dependent spatial averaging effects may be improved.

II. Methods

A. Measurements of Effective Sensitive Element Radii

Frequency-dependent effective sensitive element radii $a_{\text{eff}}(f)$ were obtained for seven needle hydrophones (Table I, last two rows) from least-squares model fits to directivity functions as described elsewhere [2], [22], [23], [24], [26], [27], [28], [29], [54]. Directivities were measured at frequencies ranging from 0.5 to 20 MHz and angles ranging from $\pm 65^\circ$ using methods previously reported from our laboratories [2], [25], [29]. By driving source transducers with sufficiently high voltage to produce nonlinear pressure waves with significant harmonic content, directivities at multiple harmonic frequencies could be measured from a single transmitted tone burst.

Directivities and frequency-dependent effective sensitive element radii were measured in two orthogonal planes, so that

TABLE I
HYDROPHONE DATASET

Reference	Hydrophone	Nominal Sensitive Element Diameter d_g (μm)	Frequency (MHz) ranges
Beard *et al.*, 2000 [22]	PA HPM075/1 PA HPM02/1	75 200	1-20 (9)
Wear *et al.*, 2018 [25]	ON HNC-0200, ON HNA-0400, ON HNP-1000	200 400 1000	1-10 (7)
Martin *et al.*, 2019 [26]	PA NH0200	200	1, 3 (2)
Wilkens *et al.*, 2023 [27]	PA NH0075, PA NH0200, PA NH0500	75 200 500	1-45 (8)
Wear, Fury, and Alvarenga., 2025 (present investigation)	PA NH0075, PA NH0200, PA NH0500, ON HNR-0500 PA NH1000	75 200 500 500 1000	1-20 (14)
Wear, Fury, and Alvarenga, 2025 (present investigation)	ON HNC-0200 ON HNP-0200	200 200	0.5, 1 (2)

ON: Onda (Sunnyvale, CA), PA: Precision Acoustics (Dorchester, U.K.). The PA HPM series hydrophones appear to be forerunners of the PA NH series. In the frequency column, the numbers in parentheses indicate the number of frequencies at which directivity and effective sensitive element size were measured for each hydrophone. Although measurements by Wilkens *et al.* were essentially continuous, measurements at eight discrete frequencies were digitized and used for the data analysis here.

means and standard deviations could be computed at all angles and frequencies.

Previous studies have shown that $a_{\text{eff}}(f)$ is primarily a function of ka_g, where $k = 2\pi/\lambda$, λ is the wavelength, and a_g is the geometrical (≈ nominal) sensitive element radius [2], [25], [29], [31]. However, the functional form depends on hydrophone type: membrane, needle, capsule, or fiber optic [2]. The ranges of frequencies and a_g for measurements listed in the last two rows of Table I result in a minimum ka_g value of 0.16.

B. Comparison With Previous Publications

The new data acquired for this investigation were pooled with data reported in four publications between 2000 and 2023 (Table I, top four rows) to enhance statistical robustness and generalizability of the resulting empirical formula for needle hydrophone spatial resolution as a function of ka_g. Data that had been published in graphical form [22], [27] were digitized using the MATLAB (Natick, MA) function GRABIT (https://www.mathworks.com/MATLABcentral/fileexchange/7173-grabit). Uncertainties of estimates of frequency-dependent effective sensitive element diameters were not available for some of these previously published studies.

To enhance relevance to modern researchers, the dataset was restricted to hydrophones manufactured by contemporary suppliers (since frequency-dependent effective sensitive element size can conceivably exhibit some dependence on needle hydrophone design). The dataset therefore excludes data from some studies based on hydrophones of unspecified origin [23], [24] or manufactured over 40 years ago by suppliers that no longer make hydrophones [21].

To provide insight into the physics of needle hydrophone sensing, empirical frequency-dependent effective sensitive element sizes were compared with predictions of the RP model [52] and the UB model [21], [53].

III. RESULTS

A. Directivity

Figs. 1 and 2 show the directivity measurements for two needle hydrophones with nominal sensitive element diameters of 200 (Fig. 1) and 500 (Fig. 2) μm. Phase cancellation of oblique plane waves at the sensitive element surface tends to increase as angle, frequency, and/or nominal sensitive element diameter increase. Therefore, directivity functions tend to decrease as any one of these three parameters increases.

Fig. 3 shows frequency-dependent standard deviations of directivity measurements averaged over all angles ($|\theta| \leq 65°$) for five hydrophones (nominal sensitive element sizes: 75–1000 μm) interrogated from 1 to 20 MHz for the new (2025) measurements (Table I, last two rows). A least-squares linear fit is also shown. Directivity standard deviation averaged over all angles, nominal sensitive element sizes, and frequencies (1–20 MHz) was 0.029 (2.9%).

B. Frequency-Dependent Effective Sensitive Element Size

The figure in the abstract shows relative difference $\Delta a/a_g$ plotted versus ka_g, where $\Delta a = a_{\text{eff}}(f) - a_g$, from all investigations listed in Table I. The data were fit to a two-parameter empirical model

$$\frac{\Delta a}{a_g} = \frac{A\exp\left(-ka_g/B\right)}{ka_g}. \tag{1}$$

The parameter values that minimized root mean squared difference (RMSD) between data and empirical model were $A = 94\%$ and $B = 5.1$. The RMSD was 36.5%. The empirical model indicates that the difference between effective and geometrical sensitive element radii is approximately 100% at $ka_g = 0.80$, which corresponds to $\lambda = 3.9d_g \approx 4d_g$.

Fig. 4 shows relative error $\Delta a/a_g$ plotted versus ka_g for Onda hydrophones interrogated in one previous [25] and one current FDA/NPL collaboration (see Table I). The empirical model ($A = 82\%$; $B = 5.1$) exhibits substantial (>15%) deviation from the RP model for $ka_g < 0.60$.

Fig. 5 shows relative error $\Delta a/a_g$ plotted versus ka_g for Precision Acoustics (PA) hydrophones reported in previous publications ("B" [22], "M" [26], and "W" [27]) and new measurements from the FDA/NPL collaboration reported here for the first time ("F") (see Table I). The empirical model ($A = 101\%$; $B = 5.1$) exhibits substantial (>15%) deviation from the RP model for $ka_g < 0.85$.

Figs. 4 and 5 offer the first empirical confirmation in needle hydrophones for a theoretical prediction that for ka_g values below the range of good agreement for the RP model, there is a range of ka_g values for which directivity functions fall between the predictions of RP and UB models [52]. Since

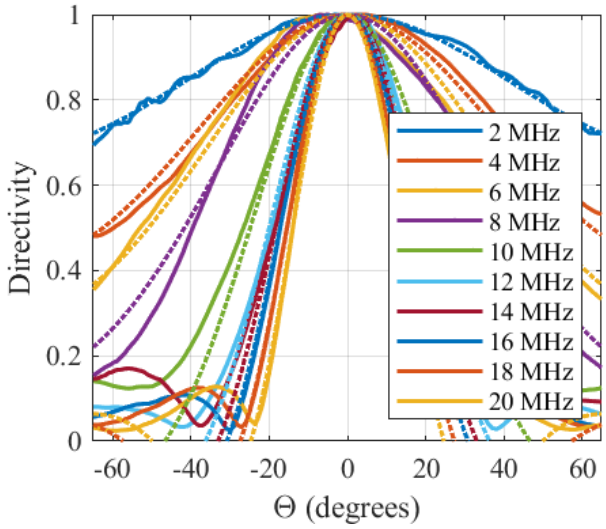

Fig. 1. Directivity for PA NH0200 hydrophone (nominal sensitive element diameter = 200 μm) measured in the present investigation. The dotted lines represent the function fits that were used in the estimation of effective sensitive element radii (see Section II-A for details).

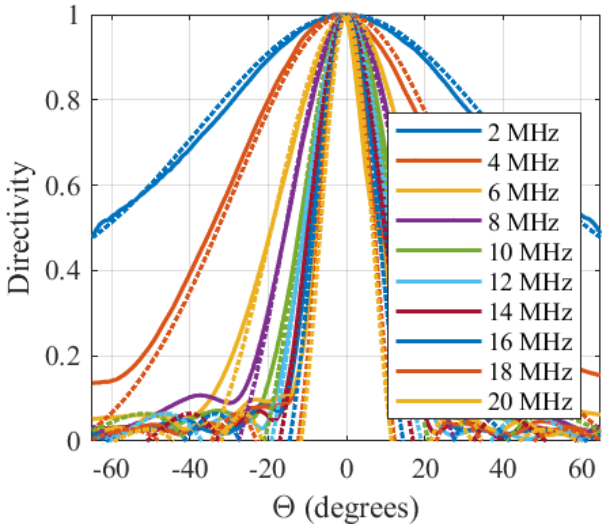

Fig. 2. Directivity for PA NH0500 hydrophone (nominal sensitive element diameter = 500 μm) measured in the present investigation. The dotted lines represent the function fits that were used in the estimation of effective sensitive element radii (see Section II-A for details).

$a_{\text{eff}}(f)$ is derived from directivity, the same would apply to $\Delta a_{\text{eff}}(f)/a_g$.

For all data from Table I and the figure in the abstract, the minimum-RMSD empirical model exhibits substantial (>15%) deviation from the RP model for $ka_g < 0.75$, which corresponds to $\lambda = 4.2d_g \approx 4d_g$.

IV. Discussion

A. Effective Sensitive Element Size and Spatial Resolution

An empirical model has been developed to predict the effective sensitive element size for needle hydrophones. The model enables researchers to estimate and report the spatial resolution of their needle hydrophone at their frequency of operation (when $ka_g \geq 0.16$).

For a hydrophone with nominal sensitive element diameter of 75 μm and a frequency of 1 MHz ($ka_g = 0.16$), the model predicts that average effective sensitive element diameter is 505 μm. For a hydrophone with a nominal sensitive element diameter of 400–500 μm and a frequency of 500 kHz (common parameters for transcranial neuromodulation in humans [39], [40], [41], [42], [43], [44], [45] and animals [39], [46], [47], [48], [49], [50], [51]; $ka_g = 0.42$–0.53 or $\lambda/d_g = 5.9$–7.4), the model predicts that average effective sensitive element diameter is 1215–1298 μm. Such enlarged effective sensitive element diameters have ramifications for spatial resolution, hydrophone spatial averaging corrections, and optimal lateral scanning increments for field mapping.

B. Model: Regime of Validity and Physical Interpretation

The RP model can predict directivity of needle and fiber optic hydrophones based on geometrical sensitive element size and frequency [52]. A previous study suggested that a set of

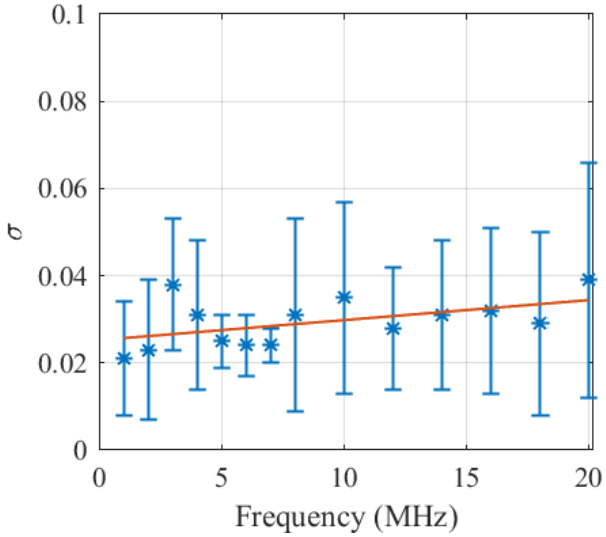

Fig. 3. Frequency-dependent standard deviations of directivity measurements averaged over angles ($|\theta| \leq 65°$) and nominal sensitive element sizes (75–1000 μm). A least-squares linear fit is also shown.

four needle hydrophones conformed well to the RP model for $ka_g \geq 0.4$ [25]. That study was conducted on three Onda hydrophones and one manufactured by the Force Technology Institute (not commercially available). The full dataset in Table I (16 hydrophones) covered the low-frequency range more extensively (down to $ka_g \geq 0.16$ instead of 0.4) and imposed a new quantitative criterion to determine conformance with the RP model (<15% deviation). The analysis presented herein implies that the regime for good agreement should be refined from $ka_g \geq 0.4$ to $ka_g \geq 0.60$ for Onda needle hydrophones and to $ka_g \geq 0.75$ for Onda and PA needle hydrophones collectively.

Figs. 6 and 7 compare the differences between experimental estimates of $a_{\text{eff}}(f)$ to RP and UB models for Onda (Fig. 6) and PA (Fig. 7) needle hydrophones. Fig. 6 shows that the

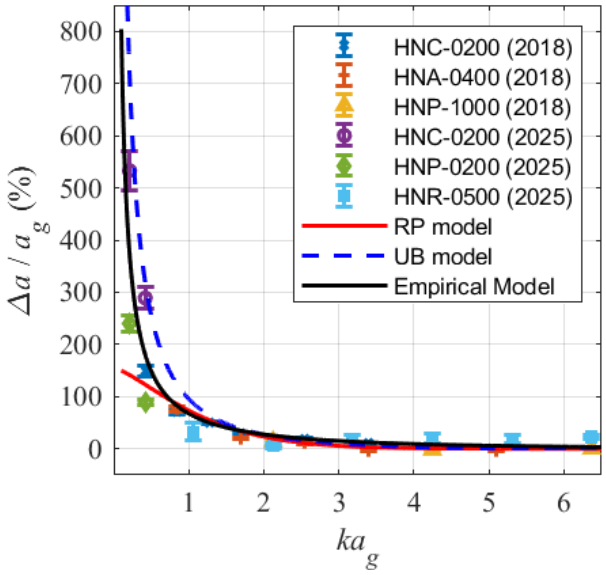

Fig. 4. Difference between effective sensitive element radii (a_{eff}) and nominal geometrical sensitive element radii (a_g) normalized to a_g for Onda hydrophones plotted versus ka_g. All data from FDA/NPL collaborations. RP: rigid piston. UB: unbaffled.

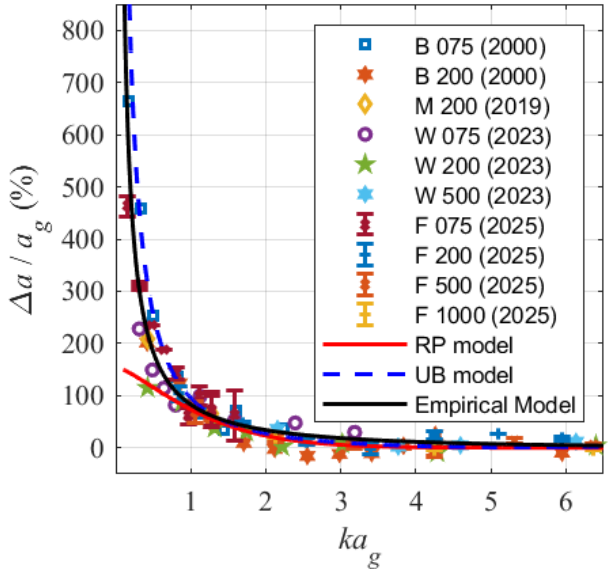

Fig. 5. Difference between effective sensitive element radii (a_{eff}) and nominal geometrical sensitive element radii (a_g) normalized to a_g for PA hydrophones plotted versus ka_g. B: Beard et al. [22] M: Martin et al. [26] W: Wilkens et al. [27] F: FDA NPL collaboration. RP: rigid piston. UB: unbaffled.

RP model conformed more closely than the UB model to empirical estimates from Onda needle hydrophones throughout the frequency range investigated. Fig. 7 suggests that the two models performed comparably for PA needle hydrophones throughout the frequency range investigated. Discrepancies in the estimates of $a_{\text{eff}}(f)$ between Onda and PA hydrophones might be attributable to differences in structure and material properties (e.g., acoustic impedance).

A previous study suggested that capsule hydrophones conform to the RP model for $ka_g \geq 0.7$ but show deviations for $0.4 \leq ka_g < 0.7$ [2]. Capsule hydrophones are similar to needle hydrophones except that they have a broader ellipsoidal base [55]. Fig. 8 shows the functional fits for relative error $\Delta a/a_g$ plotted versus ka_g for the needle hydrophones in Table I, and, for the sake of comparison, for capsule [2] and membrane [29] hydrophones reported in previous publications. The functional fits for needle and capsule hydrophones show similar conformance to the RP model for $ka_g \geq 0.7$ and similar deviations from the RP model for $ka_g < 0.7$.

Discrepancies between RP and UB model predictions and measurements of frequency-dependent effective sensitive element size might be partially attributable to ideal assumptions of theory that are not fully satisfied in practice. These can compromise the predictions of diffracted and reflected waves from the needle. First, the RP assumption neglects all elastic properties of the needle hydrophone, including penetration of sound into the needle, excitation of transverse waves in and surface waves on the needle, and resonances at discrete angles and frequencies [52]. Second, the RP and UB models assume perfect cylindrical geometry, whereas real needle hydrophones have been demonstrated to have cross sections that are more accurately described as elliptical, with measurable deviations from circular symmetry [21], [24]. Third, the RP and UB models assume uniform sensitivity across the sensitive element of

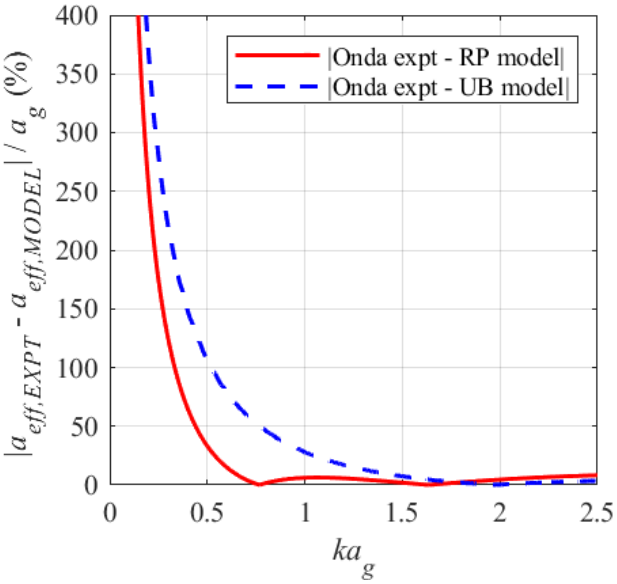

Fig. 6. Differences between experimental estimates of effective sensitive element radius $a_{\text{eff}}(f)$ to RP and UB models for Onda hydrophones. RP: rigid piston. UB: unbaffled.

the needle hydrophone. Deviations from perfect circularity can "blur" the diffracted wave, thereby reducing its amplitude [52].

In addition to predicting directivity and effective sensitive element size, RP models have been derived [52], [56] and experimentally validated [57], [58] for normally incident plane waves to predict needle and reflectance-type fiber optic hydrophone sensitivity.

C. Implications of Application of RP Model at Low Frequencies ($\lambda > 4d_g$) in Previous Investigations

Three previous publications [13], [14], [18] assumed the RP model for needle hydrophone frequency-dependent effective sensitive element size rather than the more general empirical

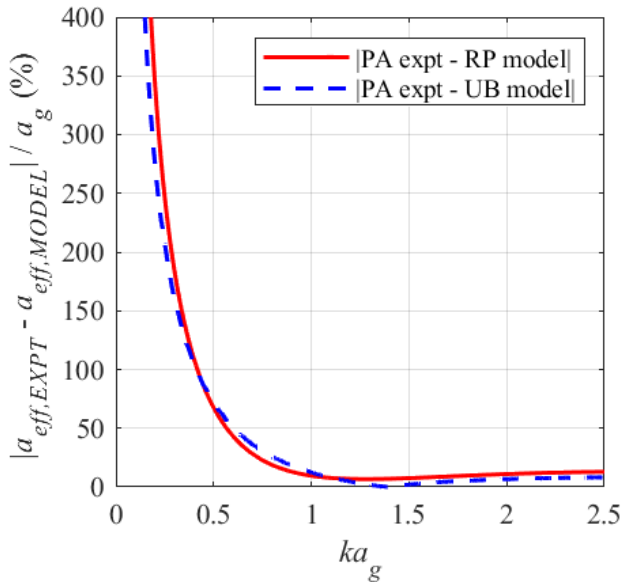

Fig. 7. Differences between experimental estimates of effective sensitive element radius $a_{\text{eff}}(f)$ to RP and UB models for PA hydrophones. RP: rigid piston. UB: unbaffled.

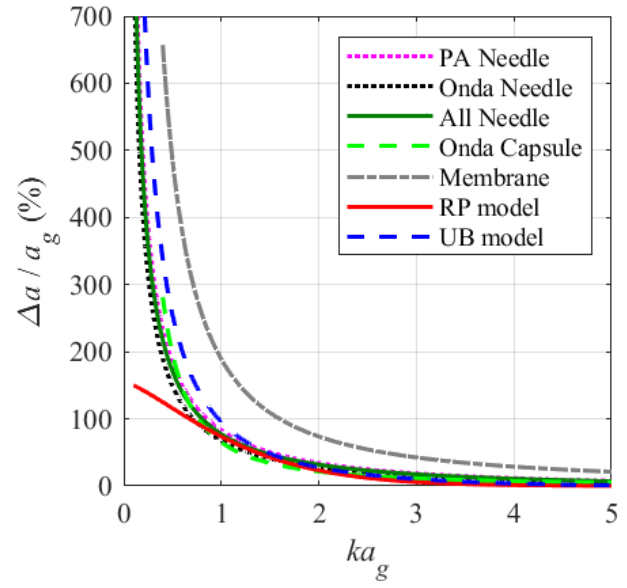

Fig. 8. Functional fits for normalized difference $\Delta a/a_g = (a_{\text{eff}} - a_g)/a_g$ between effective radii (a_{eff}) and nominal geometrical sensitive element radii (a_g). Fits are shown for PA needle hydrophones, Onda needle hydrophones, PA and Onda needle hydrophones collectively ("all needle"), Onda capsule hydrophones (from previous investigation), and multiple-vendor membrane hydrophones (from previous investigation). Two theoretical models are shown. RP: rigid piston. UB: unbaffled.

model obtained in the present investigation. As stated previously, the difference between the two models is significant for $ka_g < 0.75$. Two of the previous investigations had minimum values for ka_g of 1.06 [13] and 1.27 [14] and were therefore essentially unaffected by model choice. Another investigation had a minimum value of ka_g of 0.47 [18], but the spatial averaging effect was recomputed using [12, eqs. (20) and (21)] (which have been adopted in IEC 62127-1 [20]) and found to be identical and negligible (1%) using both models.

Three previous investigations have assumed the RP model for capsule hydrophone frequency-dependent effective sensitive element size rather than the more general empirical model obtained recently [2]. One of the previous investigations had minimum values for ka_g of 0.90 [17] and was therefore essentially unaffected by model choice. In two other studies, $ka_g = 0.36$ for the fundamental component of the nonlinear signals [15], [19]. The spatial averaging effect was recomputed using [12, eqs. (20) and (21)] to be 1% for the RP model and 4% for the more general empirical model, resulting in a small 3% difference predicted by the two models.

V. Conclusion

Spatial resolution limitations and spatial averaging artifacts for hydrophones are determined by frequency-dependent effective sensitive element diameter (which may be inferred from directivity measurements) rather than nominal or geometrical sensitive element diameter. An empirical formula, derived from directivity measurements, has been obtained to enable researchers to easily estimate and report the effective sensitive element diameter of their needle hydrophone at their operating frequency. The empirical model has a greater range of validity than the RP model ($ka_g > 0.16$ versus $ka_g > 0.75$). The frequency range was broad enough to encompass transcranial ultrasound applications (i.e., low frequencies) as well as most diagnostic and therapeutic applications. When $\lambda > 4d_g$, the effective sensitive element diameter can exceed nominal sensitive element diameter by over 100%. Needle (and capsule) hydrophones conform closely to RP theory when $\lambda < 4d_g$ and fall between RP theory and theory for an unbaffled (UB) circular piston when $\lambda > 4d_g$.

Acknowledgment

The mention of commercial products, their sources, or their use in connection with material reported herein is not to be construed as either an actual or implied endorsement of such products by the Department of Health and Human Services or the National Physical Laboratory.

References

[1] G. R. Harris et al., "Hydrophone measurements for biomedical ultrasound applications: A review," *IEEE Trans. Ultrason., Ferroelectr., Freq. Control*, vol. 70, no. 2, pp. 85–100, Feb. 2023, doi: 10.1109/TUFFC.2022.3213185.

[2] K. A. Wear and A. Shah, "Nominal versus actual spatial resolution: Comparison of directivity and frequency-dependent effective sensitive element size for membrane, needle, capsule, and fiber-optic hydrophones," *IEEE Trans. Ultrason., Ferroelectr., Freq. Control*, vol. 70, no. 2, pp. 112–119, Feb. 2023, doi: 10.1109/TUFFC.2022.3211183.

[3] *Ultrasonics—Hydrophones—Part 3: Properties of Hydrophones for Ultrasonic Fields Up to 40 MHz*, Standard 62127-3, IEC, Geneva, Switzerland, 2013.

[4] K. Beissner, "Maximum hydrophone size in ultrasonic field measurements," *Acustica*, vol. 59, pp. 61–66, Jan. 1985.

[5] R. C. Preston, D. R. Bacon, and R. A. Smith, "Calibration of medical ultrasonic equipment-procedures and accuracy assessment," *IEEE Trans. Ultrason., Ferroelectr., Freq. Control*, vol. 35, no. 2, pp. 110–121, Mar. 1988, doi: 10.1109/58.4161.

[6] R. A. Smith, "Are hydrophones of diameter 0.5 mm small enough to characterise diagnostic ultrasound equipment?" *Phys. Med. Biol.*, vol. 34, no. 11, pp. 1593–1607, Nov. 1989. [Online]. Available: https://www.ncbi.nlm.nih.gov/pubmed/2685834

[7] B. Zeqiri and A. D. Bond, "The influence of waveform distortion on hydrophone spatial-averaging corrections—Theory and measurement," *J. Acoust. Soc. Amer.*, vol. 92, no. 4, pp. 1809–1821, Oct. 1992, doi: 10.1121/1.403837.

[8] E. G. Radulescu, P. A. Lewin, A. Goldstein, and A. Nowicki, "Hydrophone spatial averaging corrections from 1 to 40 MHz," *IEEE Trans. Ultrason., Ferroelectr., Freq. Control*, vol. 48, no. 6, pp. 1575–1580, Nov. 2001, doi: 10.1109/58.971709.

[9] E. G. Radulescu, P. A. Lewin, and A. Nowicki, "1–60 MHz measurements in focused acoustic fields using spatial averaging corrections," *Ultrasonics*, vol. 40, nos. 1–8, pp. 497–501, May 2002. [Online]. Available: https://www.ncbi.nlm.nih.gov/pubmed/12159990

[10] O. Bessonova and V. Wilkens, "Investigation of spatial averaging effect of membrane hydrophones for working frequencies in the low MHz range," in *Proc. DAGA-Darmstadt*, 2012, pp. 937–938.

[11] G. Xing, P. Yang, P. Hu, K. H. Lam, L. He, and Z. Zhang, "Field characterization of steady state focused transducers using hydrophones based on Fresnel approximation," *Meas. Sci. Technol.*, vol. 28, no. 6, Jun. 2017, Art. no. 065005, doi: 10.1088/1361-6501/aa6421.

[12] K. A. Wear, "Considerations for choosing sensitive element size for needle and fiber-optic hydrophones—Part I: Spatiotemporal transfer function and graphical guide," *IEEE Trans. Ultrason., Ferroelectr., Freq. Control*, vol. 66, no. 2, pp. 318–339, Feb. 2019, doi: 10.1109/TUFFC.2018.2886067.

[13] K. A. Wear and Y. Liu, "Considerations for choosing sensitive element size for needle and fiber-optic hydrophones—Part II: Experimental validation of spatial averaging model," *IEEE Trans. Ultrason., Ferroelectr., Freq. Control*, vol. 66, no. 2, pp. 340–347, Feb. 2019, doi: 10.1109/TUFFC.2018.2886071.

[14] K. A. Wear and S. M. Howard, "Correction for spatial averaging artifacts in hydrophone measurements of high-intensity therapeutic ultrasound: An inverse filter approach," *IEEE Trans. Ultrason., Ferroelectr., Freq. Control*, vol. 66, no. 9, pp. 1453–1464, Sep. 2019, doi: 10.1109/TUFFC.2019.2924351.

[15] K. A. Wear, A. Shah, and C. Baker, "Correction for hydrophone spatial averaging artifacts for circular sources," *IEEE Trans. Ultrason., Ferroelectr., Freq. Control*, vol. 67, no. 12, pp. 2674–2691, Dec. 2020, doi: 10.1109/TUFFC.2020.3007808.

[16] K. A. Wear, "Hydrophone spatial averaging correction for acoustic exposure measurements from arrays—Part I: Theory and impact on diagnostic safety indexes," *IEEE Trans. Ultrason., Ferroelectr., Freq. Control*, vol. 68, no. 3, pp. 358–375, Mar. 2021, doi: 10.1109/TUFFC.2020.3037946.

[17] K. A. Wear, A. Shah, A. M. Ivory, and C. Baker, "Hydrophone spatial averaging correction for acoustic exposure measurements from arrays—Part II: Validation for ARFI and pulsed Doppler waveforms," *IEEE Trans. Ultrason., Ferroelectr., Freq. Control*, vol. 68, no. 3, pp. 376–388, Mar. 2021, doi: 10.1109/TUFFC.2020.3037999.

[18] K. A. Wear, "Spatiotemporal deconvolution of hydrophone response for linear and nonlinear beams—Part I: Theory, spatial-averaging correction formulas, and criteria for sensitive element size," *IEEE Trans. Ultrason., Ferroelectr., Freq. Control*, vol. 69, no. 4, pp. 1243–1256, Apr. 2022, doi: 10.1109/TUFFC.2022.3150186.

[19] K. A. Wear, A. Shah, and C. Baker, "Spatiotemporal deconvolution of hydrophone response for linear and nonlinear beams—Part II: Experimental validation," *IEEE Trans. Ultrason., Ferroelectr., Freq. Control*, vol. 69, no. 4, pp. 1257–1267, Apr. 2022, doi: 10.1109/TUFFC.2022.3150179.

[20] *Ultrasonics—Hydrophones—Part 1: Measurement and Characterization of Medical Ultrasonic Fields*, Standard 62127-1, IEC, Geneva, Switzerland, 2022.

[21] D. G. Shombert, S. W. Smith, and G. R. Harris, "Angular response of miniature ultrasonic hydrophones," *Med. Phys.*, vol. 9, no. 4, pp. 484–492, Jul. 1982, doi: 10.1118/1.595114.

[22] P. C. Beard, A. M. Hurrell, and T. N. Mills, "Characterization of a polymer film optical fiber hydrophone for use in the range 1 to 20 MHz: A comparison with PVDF needle and membrane hydrophones," *IEEE Trans. Ultrason., Ferroelectr., Freq. Control*, vol. 47, no. 1, pp. 256–264, Jan. 2000, doi: 10.1109/58.818769.

[23] E. G. Radulescu, P. A. Lewin, A. Nowicki, and W. A. Berger, "Hydrophones' effective diameter measurements as a quasi-continuous function of frequency," *Ultrasonics*, vol. 41, no. 8, pp. 635–641, Nov. 2003, doi: 10.1016/s0041-624x(03)00180-x.

[24] M. Yoshioka, "Difference between nominal and measured active element sizes of hydrophones," *Jpn. J. Appl. Phys.*, vol. 47, no. 5S, pp. 3926–3928, May 2008.

[25] K. A. Wear, C. Baker, and P. Miloro, "Directivity and frequency-dependent effective sensitive element size of needle hydrophones: Predictions from four theoretical forms compared with measurements," *IEEE Trans. Ultrason., Ferroelectr., Freq. Control*, vol. 65, no. 10, pp. 1781–1788, Oct. 2018, doi: 10.1109/TUFFC.2018.2855967.

[26] E. Martin and B. Treeby, "Investigation of the repeatability and reproducibility of hydrophone measurements of medical ultrasound fields," *J. Acoust. Soc. Amer.*, vol. 145, no. 3, pp. 1270–1282, Mar. 2019, doi: 10.1121/1.5093306.

[27] V. Wilkens and M. Weber, "Determination of effective hydrophone sizes from 1 to 50 MHz according to IEC 62127-3:2022 using short pulse excitation," in *Proc. IEEE Int. Ultrason. Symp. (IUS)*, Sep. 2023, pp. 1–4, doi: 10.1109/IUS51837.2023.10307039.

[28] V. Wilkens and W. Molkenstruck, "Broadband PVDF membrane hydrophone for comparisons of hydrophone calibration methods up to 140 MHz," *IEEE Trans. Ultrason., Ferroelectr., Freq. Control*, vol. 54, no. 9, pp. 1784–1791, Sep. 2007, doi: 10.1109/TUFFC.2007.462.

[29] K. A. Wear, C. Baker, and P. Miloro, "Directivity and frequency-dependent effective sensitive element size of membrane hydrophones: Theory versus experiment," *IEEE Trans. Ultrason., Ferroelectr., Freq. Control*, vol. 66, no. 11, pp. 1723–1730, Nov. 2019, doi: 10.1109/TUFFC.2019.2930042.

[30] B. Cox and P. Beard, "The frequency-dependent directivity of a planar Fabry–Pérot polymer film ultrasound sensor," *IEEE Trans. Ultrason., Ferroelectr., Freq. Control*, vol. 54, no. 2, pp. 394–404, Feb. 2007, doi: 10.1109/TUFFC.2007.253.

[31] K. A. Wear and S. M. Howard, "Directivity and frequency-dependent effective sensitive element size of a reflectance-based fiber-optic hydrophone: Predictions from theoretical models compared with measurements," *IEEE Trans. Ultrason., Ferroelectr., Freq. Control*, vol. 65, no. 12, pp. 2343–2348, Dec. 2018, doi: 10.1109/TUFFC.2018.2872840.

[32] J. White, G. T. Clement, and K. Hynynen, "Transcranial ultrasound focus reconstruction with phase and amplitude correction," *IEEE Trans. Ultrason., Ferroelectr., Freq. Control*, vol. 52, no. 9, pp. 1518–1522, Sep. 2005. [Online]. Available: https://www.ncbi.nlm.nih.gov/pubmed/16285450

[33] W. J. Elias et al., "A pilot study of focused ultrasound thalamotomy for essential tremor," *New England J. Med.*, vol. 369, no. 7, pp. 640–648, Aug. 2013, doi: 10.1056/nejmoa1300962.

[34] E. E. Konofagou, "Optimization of the ultrasound-induced blood-brain barrier opening," *Theranostics*, vol. 2, no. 12, pp. 1223–1237, 2012, doi: 10.7150/thno.5576.

[35] E. E. Konofagou, "Trespassing the barrier of the brain with ultrasound," *Acoust. Today*, vol. 13, no. 4, pp. 21–26, 2017.

[36] D. McMahon, M. A. O'Reilly, and K. Hynynen, "Therapeutic agent delivery across the blood–brain barrier using focused ultrasound," *Annu. Rev. Biomed. Eng.*, vol. 23, no. 1, pp. 89–113, Jul. 2021, doi: 10.1146/annurev-bioeng-062117-121238.

[37] E. Martin, J.-F. Aubry, M. Schafer, L. Verhagen, B. Treeby, and K. B. Pauly, "ITRUSST consensus on standardised reporting for transcranial ultrasound stimulation," *Brain Stimulation*, vol. 17, no. 3, pp. 607–615, May 2024, doi: 10.1016/j.brs.2024.04.013.

[38] J. L. B. Robertson, B. T. Cox, J. Jaros, and B. E. Treeby, "Accurate simulation of transcranial ultrasound propagation for ultrasonic neuromodulation and stimulation," *J. Acoust. Soc. Amer.*, vol. 141, no. 3, pp. 1726–1738, Mar. 2017, doi: 10.1121/1.4976339.

[39] W. Legon et al., "Transcranial focused ultrasound modulates the activity of primary somatosensory cortex in humans," *Nature Neurosci.*, vol. 17, no. 2, pp. 322–329, Feb. 2014, doi: 10.1038/nn.3620.

[40] W. Legon, L. Ai, P. Bansal, and J. K. Mueller, "Neuromodulation with single-element transcranial focused ultrasound in human thalamus," *Human Brain Mapping*, vol. 39, no. 5, pp. 1995–2006, May 2018, doi: 10.1002/hbm.23981.

[41] L. Ai, P. Bansal, J. K. Mueller, and W. Legon, "Effects of transcranial focused ultrasound on human primary motor cortex using 7T fMRI: A pilot study," *BMC Neurosci.*, vol. 19, no. 1, p. 56, Sep. 2018, doi: 10.1186/s12868-018-0456-6.

[42] W. Legon, P. Bansal, R. Tyshynsky, L. Ai, and J. K. Mueller, "Transcranial focused ultrasound neuromodulation of the human primary motor cortex," *Sci. Rep.*, vol. 8, no. 1, p. 10007, Jul. 2018, doi: 10.1038/s41598-018-28320-1.

[43] K. Yu, C. Liu, X. Niu, and B. He, "Transcranial focused ultrasound neuromodulation of voluntary movement-related cortical activity in humans," *IEEE Trans. Biomed. Eng.*, vol. 68, no. 6, pp. 1923–1931, Jun. 2021, doi: 10.1109/TBME.2020.3030892.

[44] C. R. Butler et al., "Transcranial ultrasound stimulation to human middle temporal complex improves visual motion detection and modulates electrophysiological responses," *Brain Stimulation*, vol. 15, no. 5, pp. 1236–1245, Sep. 2022, doi: 10.1016/j.brs.2022.08.022.

[45] M. Chen et al., "Numerical and experimental evaluation of low-intensity transcranial focused ultrasound wave propagation using human skulls for brain neuromodulation," *Med. Phys.*, vol. 50, no. 1, pp. 38–49, Jan. 2023, doi: 10.1002/mp.16090.

[46] J. K. Mueller, L. Ai, P. Bansal, and W. Legon, "Computational exploration of wave propagation and heating from transcranial focused ultrasound for neuromodulation," *J. Neural Eng.*, vol. 13, no. 5, Oct. 2016, Art. no. 056002, doi: 10.1088/1741-2560/13/5/056002.

[47] P.-C. Tsai, H. S. Gougheri, and M. Kiani, "Skull impact on the ultrasound beam profile of transcranial focused ultrasound stimulation," in *Proc. 41st Annu. Int. Conf. IEEE Eng. Med. Biol. Soc. (EMBC)*, Jul. 2019, pp. 5188–5191, doi: 10.1109/EMBC.2019.8857269.

[48] G. Lu et al., "Transcranial focused ultrasound for noninvasive neuromodulation of the visual cortex," *IEEE Trans. Ultrason., Ferroelectr., Freq. Control*, vol. 68, no. 1, pp. 21–28, Jan. 2021, doi: 10.1109/TUFFC.2020.3005670.

[49] K. Yu, X. Niu, E. Krook-Magnuson, and B. He, "Intrinsic functional neuron-type selectivity of transcranial focused ultrasound neuromodulation," *Nature Commun.*, vol. 12, no. 1, p. 2519, May 2021, doi: 10.1038/s41467-021-22743-7.

[50] C. Liu, K. Yu, X. Niu, and B. He, "Transcranial focused ultrasound enhances sensory discrimination capability through somatosensory cortical excitation," *Ultrasound Med. Biol.*, vol. 47, no. 5, pp. 1356–1366, May 2021, doi: 10.1016/j.ultrasmedbio.2021.01.025.

[51] X. Niu, K. Yu, and B. He, "Transcranial focused ultrasound induces sustained synaptic plasticity in rat hippocampus," *Brain Stimulation*, vol. 15, no. 2, pp. 352–359, Mar. 2022, doi: 10.1016/j.brs.2022.01.015.

[52] J. F. Krücker, A. Eisenberg, M. Krix, R. Lötsch, M. Pessel, and H.-G. Trier, "Rigid piston approximation for computing the transfer function and angular response of a fiber-optic hydrophone," *J. Acoust. Soc. Amer.*, vol. 107, no. 4, pp. 1994–2003, Apr. 2000.

[53] B. Delannoy, H. Lasota, C. Bruneel, R. Torguet, and E. Bridoux, "The infinite planar baffles problem in acoustic radiation and its experimental verification," *J. Appl. Phys.*, vol. 50, no. 8, pp. 5189–5195, Aug. 1979, doi: 10.1063/1.326656.

[54] G. D. Harris and D. G. Shombert, "A pulsed near-field technique for measuring the directional characteristics of acoustic receivers," *IEEE Trans. Sonics Ultrason.*, vol. SU-32, no. 6, pp. 802–808, Nov. 1985.

[55] A. R. Selfridge and P. G. Goetz, "Ellipsoidal hydrophone with improved characteristics," in *Proc. IEEE Int. Ultrason. Symp.*, Apr. 1999, pp. 1181–1184.

[56] D. S. Jones, "The scattering of a scalar wave by a semi-infinite rod of circular cross section," *Philos T R Soc S-A*, vol. 247, no. 934, pp. 499–528, 1955, doi: 10.1098/rsta.1955.0004.

[57] G. R. Harris and P. M. Gammell, "Sensitivity measurements of piezoelectric polymer hydrophones from 0.2–2 MHz using a broadband-pulse technique," *J. Acoust. Soc. Amer.*, vol. 105, no. 2, pp. 725–731, Feb. 1999, doi: 10.1121/1.426263.

[58] K. A. Wear, Y. Liu, and G. R. Harris, "Pressure pulse distortion by needle and fiber-optic hydrophones due to nonuniform sensitivity," *IEEE Trans. Ultrason., Ferroelectr., Freq. Control*, vol. 65, no. 2, pp. 137–148, Feb. 2018, doi: 10.1109/TUFFC.2017.2778566.

Keith A. Wear (Life Fellow, IEEE) received the B.A. degree in applied physics from the University of California at San Diego, San Diego, CA, USA, and the M.S. and Ph.D. degrees in applied physics, with the Ph.D. degree minor in electrical engineering, from Stanford University, Stanford, CA.

He was a Postdoctoral Research Fellow with the Physics Department, Washington University, St. Louis, MO, USA. He is currently a Research Physicist with the U.S. Food and Drug Administration, Silver Spring, MD, USA. His research interests include hydrophone measurement methodology, high-intensity therapeutic ultrasound, photoacoustics, and quantitative ultrasound.

Dr. Wear is a Fellow of the Acoustical Society of America, the American Institute for Medical and Biological Engineering, and the American Institute of Ultrasound in Medicine (AIUM). He received the 2019 AIUM Joseph H. Holmes Basic Science Pioneer Award. He received the 2026 UFFC Society Ultrasonics Distinguished Lecturer Award (https://ieee-uffc.org/distinguished-lecturer-award). He served as an Associate Editor-in-Chief for IEEE TRANSACTIONS ON ULTRASONICS, FERROELECTRICS, AND FREQUENCY CONTROL (IEEE-TUFFC) from 2019 to 2021. He has served as an Associate Editor for IEEE-TUFFC (2002–2021 and since 2025), *Journal of the Acoustical Society of America* (since 2012), and *Ultrasonic Imaging* (2013–2024). Since 2024, he has been on the Editorial Board for IEEE ACCESS. He was the Technical Program Chair of the 2008 IEEE International Ultrasonics Symposium (IUS), Beijing, China. He was the General Program Chair of the 2017 IEEE IUS, Washington, DC, USA. He has served as the Chair for the AIUM Technical Standards Committee from 2014 to 2016, AIUM Bioeffects Committee from 2021 to 2023, AIUM Basic Science and Instrumentation Community from 2004 to 2006 and from 2014 to 2016, and AIUM Therapeutic Ultrasound Community from 2013 to 2015. He is the Chair of the American Association of Physicists in Medicine Task Group 333 on Magnetic Resonance Guided Focused Ultrasound Quality Assurance. He served as an Invited Instructor in seven short courses at the IEEE IUS involving hydrophone measurement methodology in 2007, 2010, 2012, 2013, and 2023–2025. He served on the IEEE UFFC Administrative Committee from 2016 to 2018 and Ultrasonics Committee from 2015 to 2019.

Christopher R. Fury was born in Pontypool, Wales, U.K. He received the B.Sc. degree in physics from the University of Exeter, Exeter, U.K., in 2009, the M.Sc. degree in fusion energy from the University of York, York, U.K., in 2010, and the Ph.D. degree in physics from the University College London, London, U.K., in 2016.

From 2012 to 2015, he was involved with a joint project at the National Physical Laboratory (NPL), Teddington, U.K., on the characterization of ultrasound contrast agents as part of his Ph.D. studies. In 2015, he joined NPL full time and is currently a Senior Scientist working in the medical ultrasound area. His main area of work is in the primary calibration and traceability of ultrasound hydrophones, overseeing both the primary standard and secondary dissemination methods. He is further involved with acoustic field characterization methods and the measurement of hydrophone properties.

Dr. Fury is a member of the Institute of Physics (IoP), a participant in EURAMET TC-AUV-SC-U, and in IEC TC 87 working groups related to hydrophone measurement.

Andre V. Alvarenga was born in Brazil, in 1971. He received the M.Sc. and D.Sc. degrees in biomedical engineering from the Federal University of Rio de Janeiro, Rio de Janeiro, Brazil, in 1999 and 2005, respectively.

From 2005 to 2022, he worked at the National Institute of Metrology, Quality, and Technology (Inmetro), Rio de Janeiro. His work involved developing and implementing measurement techniques for ultrasonic power and acoustic properties of materials, as well as supervising graduate students. In 2013, he completed a Postdoctoral Research Fellowship at the Physikalisch-Technische Bundesanstalt (PTB), Brunswick, Germany, focusing on noninvasive temperature estimation using ultrasound imaging. Since 2022, he has been a Senior Scientist with the Ultrasound and Underwater Acoustics (UUA) Group, National Physical Laboratory (NPL), Teddington, U.K. His current responsibilities include providing measurement services for ultrasound field characterization, developing a metrological infrastructure in elastography, and advancing ultrasound metrology.

Dr. Alvarenga is a member of the International Electrotechnical Commission (IEC) Technical Committee 87 on Ultrasonics, where he contributed to Working Group 08 on ultrasonic field measurement, and a member of the Institute of Physics (IoP). His contributions to the field have been recognized through numerous publications and collaborative research projects, including initiatives supported by Innovate UK.